# Supporting Information

# UV curing polyurethane-acrylate composites as full filled thermal interface materials

Yamin Che,[a,b] Cui Liu,[a,c] Nian Li,[a,c] Wei Guo,[a,b] Min Xi,[a,c] Shudong Zhang,[a,c*] and

Zhenyang Wang[a,c*]

[a] Institute of Solid State Physics, Hefei Institutes of Physical Science, Chinese

Academy of Sciences, Hefei, Anhui, 230031, China.

[b] Department of Chemistry, University of Science and Technology of China, Hefei

   230026, China.

[c] Key Laboratory of Photovoltaic and Energy Conservation Materials, Hefei Institutes

of Physical Science, Chinese Academy of Sciences, Hefei, 230031, China.

## Corresponding Author

*Email: sdzhang@iim.ac.cn (Shudong Zhang)
*Email: zywang@iim.ac.cn (Zhenyang Wang)

# Table of Contents

Characterization results of the hBN@PEI-Cu NWs/PUA composites. (a) FTIR spectra of the pure PUA film and the hBN@PEI-Cu NWs/PUA composites. (b) XRD pattern of the hBN@PEI/Cu NWs/PUA composites. (c) TGA curves of composites with the different loading of hBN@PEI-Cu NWs filler (hBN@PEI-Cu NWs filler mass ratio: 50:1).

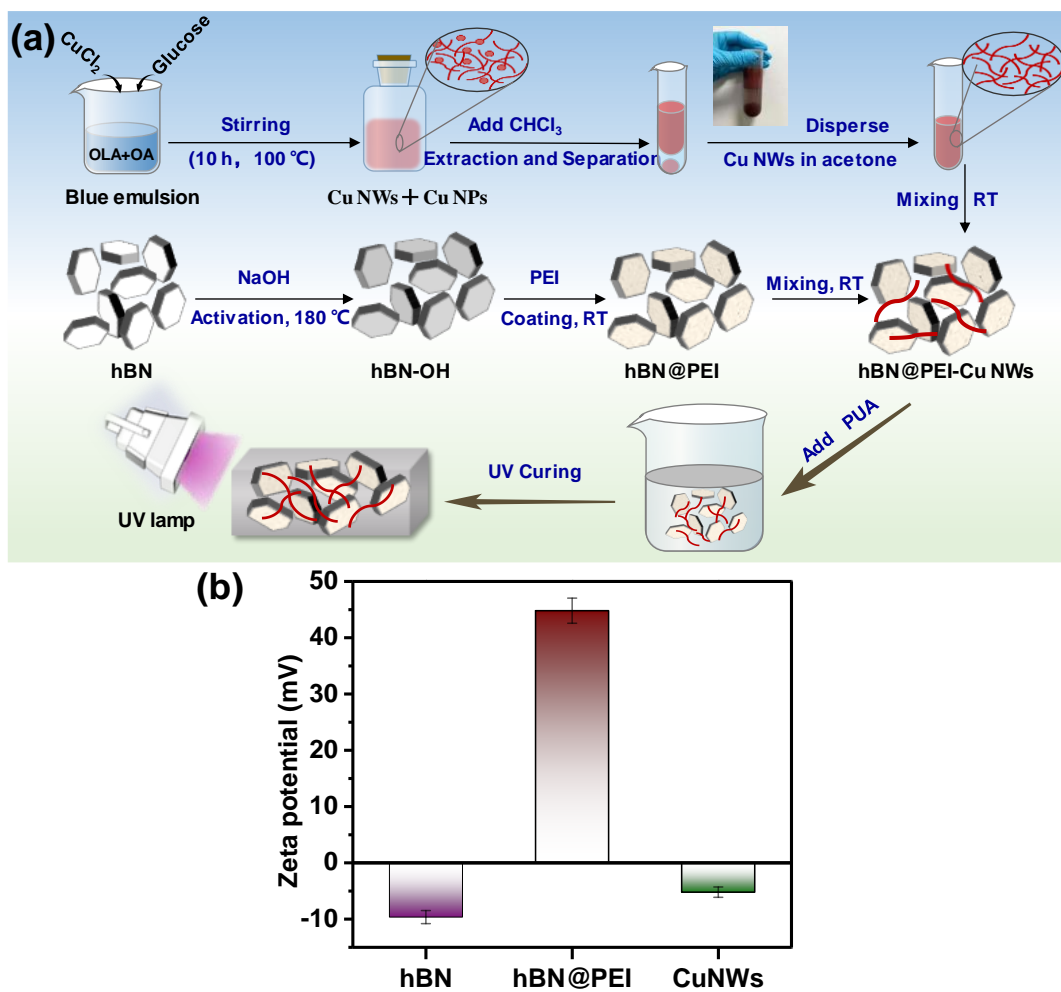Comparison of thermal conductivity of BN filled or PUA based composites previously reported.

**Figure S1.** (a) Schematic illustration of the preparation process of the hBN@PEI-Cu NWs/PUA composites. (b) Zeta potential of hBN, hBN@PEI and Cu NWs.
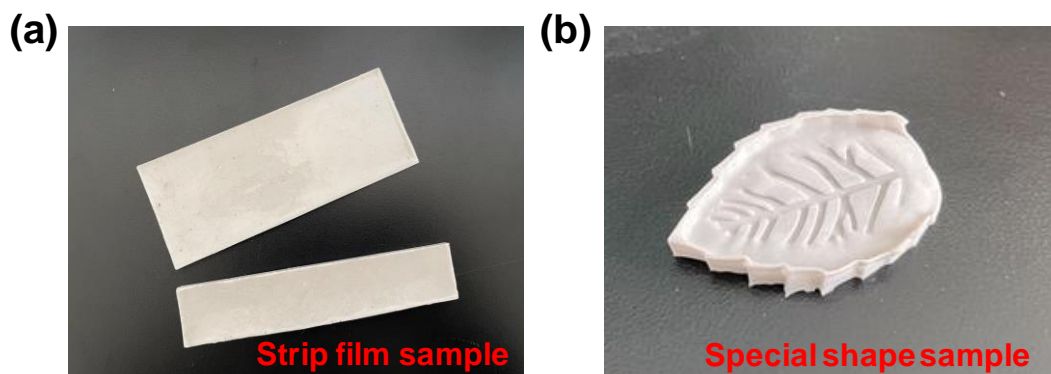


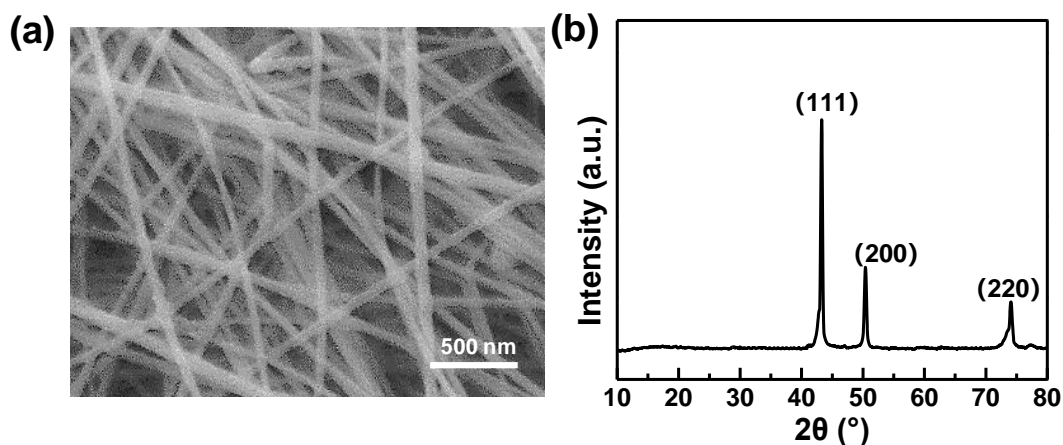**Figure S2.** Digital pictures of samples with different shapes.

**Figure S3.** (a) SEM images of Cu NWs. (b) XRD pattern of Cu NWs.

The SEM image of the obtained Cu NWs is shown in Fig. S3(a) and Fig. S3(b) shows the XRD pattern of Cu NWs, the typical diffraction peaks at $2\theta = 43.5°$, $50.8°$, and $74.4°$, corresponding to the diffractions from (111), (200), and (220) planes of face-centered cubic copper (JCPDS 065-9743), respectively.
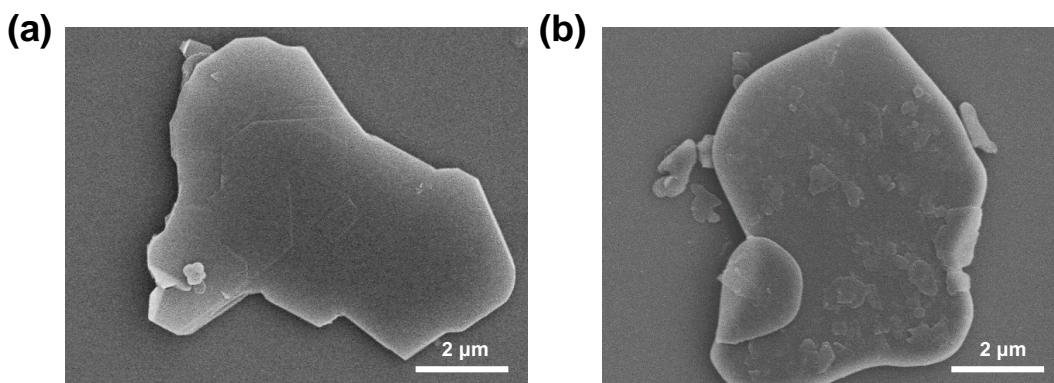


**Figure S4.** SEM images of (a) hBN and (b) hBN@PEI.

Here, the typical SEM images are shown in Fig. S4(a) and (b). After hydroxylation treatment and PEI coating, the surface of hBN microsheets become rough.
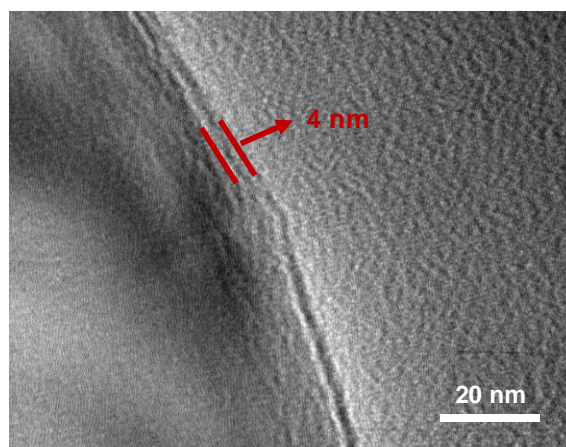
**Figure S5.** TEM images of hBN@PEI.
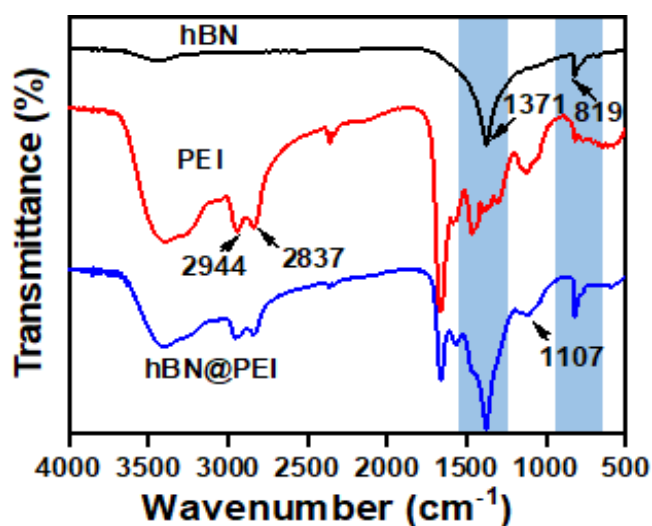


**Figure S6.** FTIR spectra of hBN, PEI and hBN@PEI.

FTIR spectra of the hBN, PEI and hBN@PEI are shown in Fig. S6. For the hBN, the peaks at 819 cm$^{-1}$ and 1371 cm$^{-1}$ are attributed to the out-of-plane bending vibration of the B-N-B bond and the in-plane stretching vibration of the B-N bond. After the coating of PEI, there are some new peaks appeared, the peaks at 2837 cm$^{-1}$ and 2944 cm$^{-1}$ attributes to the C-H vibration, and the peak at 1107 cm$^{-1}$ attributed to the C–N stretching vibration, which also appears in the FIIR spectra of PEI.

**Figure S7.** XRD patterns of hBN and hBN@PEI.



**Figure S8.** TGA curves of hBN and hBN@PEI.

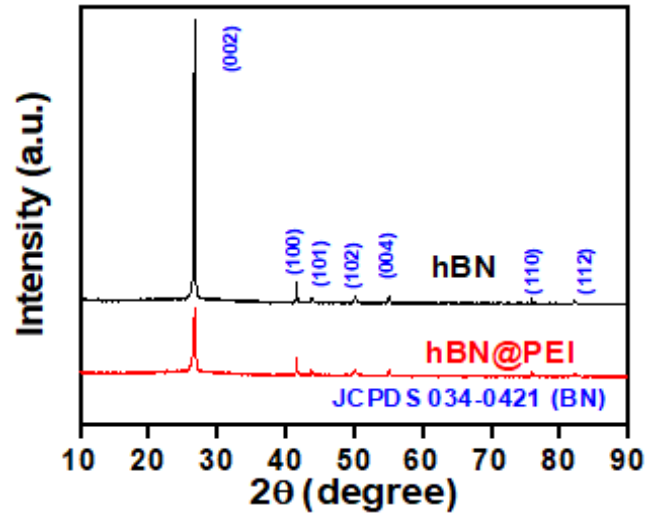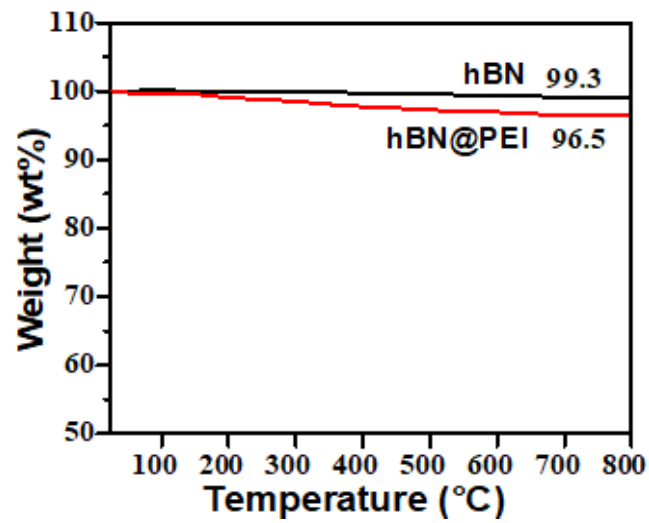Fig. S8 shows the results of the TGA test of the hBN and hBN@PEI. hBN@PEI start to decompose at 200 ℃ and the mass loss of hBN@PEI reaches 3.5wt% when heats to 800 ℃, which is the result of PEI decomposition.
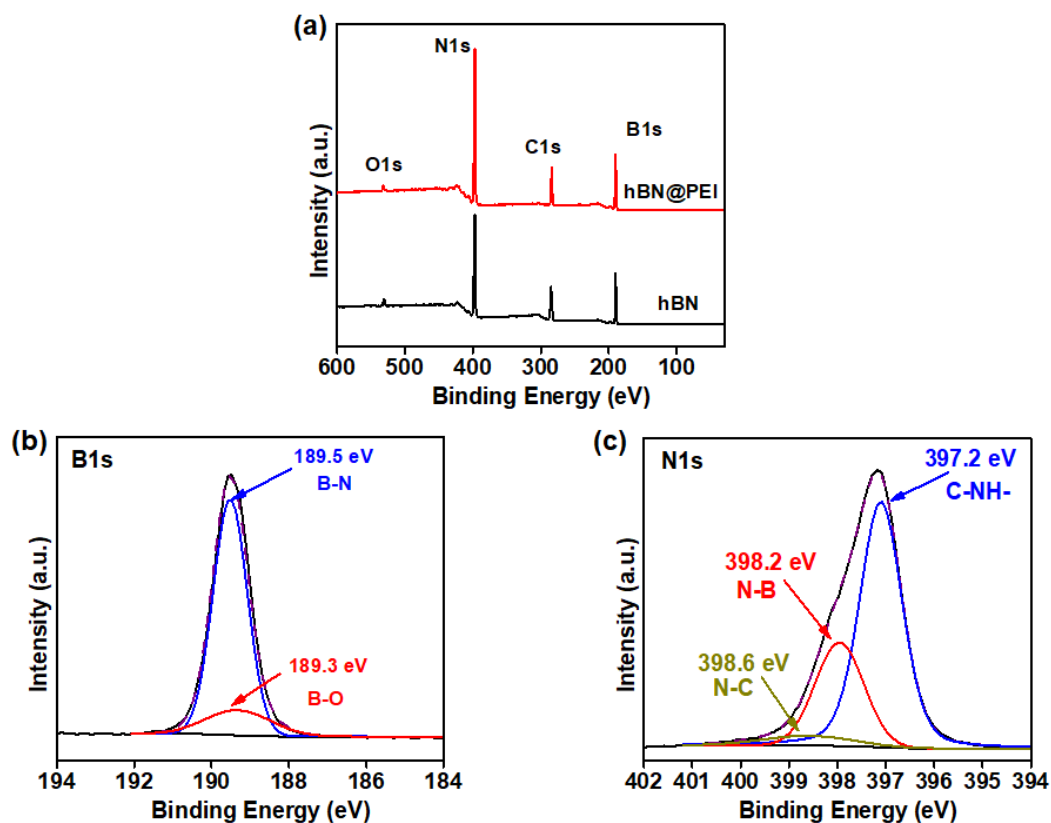
**Figure S9.** XPS spectra of hBN and hBN@PEI.

The C 1s, O 1s, B 1s and N 1s elements are seen both in the XPS survey spectra of hBN and hBN@PEI (Fig. S9a). The high-resolution B1s spectra of hBN@PEI (Fig. S9b) can be deconvoluted into two major peaks located at 189.3 and 189.5 eV, which are allocated to B-O and B-N bonds,[1] while the B–O bond maybe caused by the hydroxylation process. For the N1s spectra of hBN@PEI (Fig. S9c), three peaks at 397.2, 398.2 and 398.6 eV are been seen, which corresponds to the N-C, N-B and C-NH- bonds, respectively. Among them, the presence of N-C and C-NH- bonds is originated from the PEI.[2]
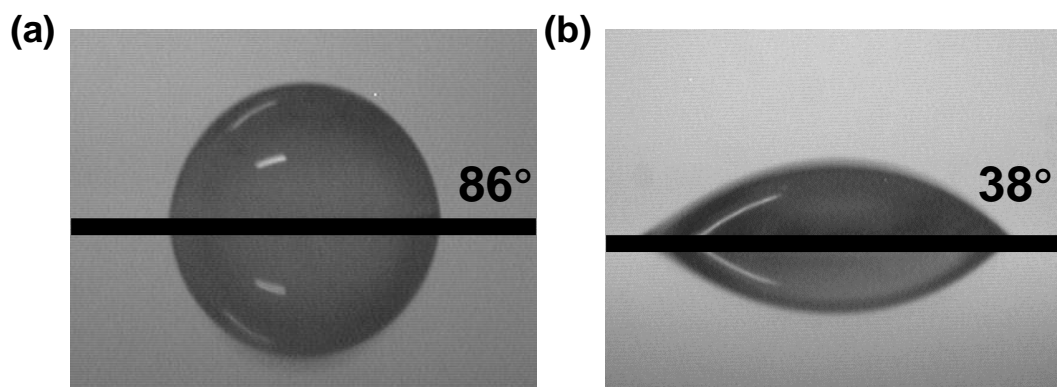
**Figure S10.** The contact angle of (a) hBN and (b) hBN@PEI.

Wettability of raw hBN and hBN@PEI were investigated by measuring its water contact angle with a sessile drop method. The raw hBN showing high contact angle of 86° indicates that it is not easy to wet solids and is in a more hydrophobic state. After being treated by PEI, the contact angle decreased to 38°, indicating a shift to hydrophilic and pave an excellent surface states for the further use.
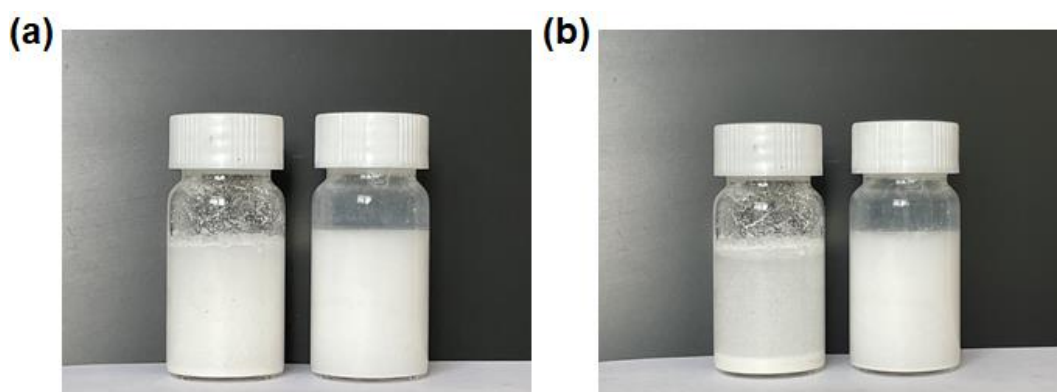


**Fig. S11.** Photos showing the difference of dispersibility of the hBN (left) and hBN@PEI (right) in water: (a) after 10 min of ultrasonication and intensely shaking. (b) after sitting for 30 min.

**Figure S12.** Characterization results of the hBN@PEI-Cu NWs/PUA composites. (a) FTIR spectra of the pure PUA film and the hBN@PEI-Cu NWs/PUA composites. (b) XRD pattern of the hBN@PEI/Cu NWs/PUA composites. (c) TGA curves of the composites with the different loading of hBN@PEI-Cu NWs filler (hBN@PEI-Cu NWs filler mass ratio: 50:1).

**Table S1.** Comparison of thermal conductivity of BN filled or PUA based composites previously reported.

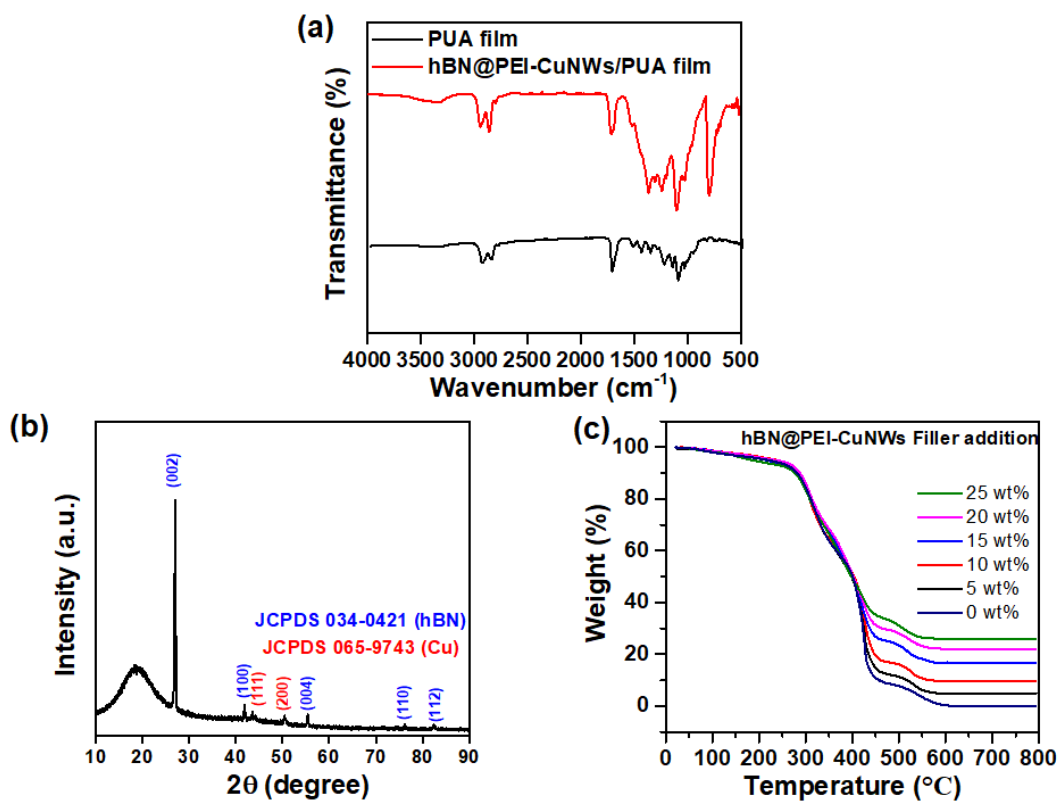| Filler type | TC (W/m·K) | Loading (filler 1/filler 2/ filler 3) | Matrix | Refs. |
|---|---|---|---|---|
| hBN | 0.729 | 20 wt% | Epoxy | [3] |
| hBN | 0.634 | 30 wt% | PVDF | [4] |
| hBN (μm/nm sized) | 1.2 | 30 wt% | PI | [5] |
| hBN/AlN | 1.449 | 12/60 wt% | Epoxy | [6] |
| hBN/MWCNT | 1.74 | 50/1 wt% | PPS | [7] |
| hBN/CNT | 0.84 | 25/2 wt% | Epoxy | [8] |
| hBN@CNT@GNP | 1.42 | 20/1/1 wt% | PC | [9] |
| hBN/Gr | 0.662 | 20/20 wt% | Epoxy | [10] |
| Ag@hBN | 0.8 | 20 wt% | Phthalonitrile | [11] |
| Ag-BNNS/Ag NWs | 0.804 | 4.7 vol%/40 wt% | Epoxy | [12] |
| hBN@2Cu | 1.049 | 25 wt% | Polybenzoxazine | [13] |
| hBN@(Ag/Cu) | 1.5645 | 25 vol% | PDMS | [14] |
| hBN@Fe | 0.99 | 30 wt% | Epoxy | [15] |
| AlN | 1.43 | 30 wt% | PUA | [16] |
| h-BN-Cu NWs | 1.535 | 20 wt% | PUA | This work |

# References

1.  B. Wang, H. Ji, X. Zhang and X. Qu, *RSC Adv.*, 2021, **11**, 38374-38382.
2.  Y. Wu, Y. He, T. Zhou, C. Chen, F. Zhong, Y. Xia, P. Xie and C. Zhang, *Prog. Org. Coat.*, 2020, **142**, 105541.
3.  M. Awais, X. Chen, C. Dai, Q. Wang, F.-B. Meng, Z. Hong, A. Paramane and Y. Tanaka, *Nanotechnology*, 2022, **33**, 135705.
4.  Q. Song, W. Zhu, Y. Deng, D. He and J. Feng, *Compos. Sci. Technol.*, 2018, **168**, 381-387.
5.  T.-L. Li and S. L.-C. Hsu, *J. Phys. Chem. B*, 2010, **114**, 6825-6829.
6.  T. Yao, K. Chen, T. Shao, C. Zhang, C. Zhang and Y. Yang, *IEEE Trans. Dielectr. Electr. Insul.*, 2020, **27**, 528-534.
7.  S. Y. Pak, H. M. Kim, S. Y. Kim and J. R. Youn, *Carbon*, 2012, **50**, 4830-4838.
8.  Y. Li, X. Tian, W. Yang, Q. Li, L. Hou, Z. Zhu, Y. Tang, M. Wang, B. Zhang, T. Pan and Y. Li, *Chem. Eng. J.,* 2019, **358**, 718-724.
9.  X. Jin, J. Wang, L. Dai, W. Wang and H. Wu, *Compos. Sci. Technol.,* 2019, **184**, 107862.
10. R. Kumar, S. K. Nayak, S. Sahoo, B. P. Panda, S. Mohanty and S. K. Nayak, *J. Mater. Sci.: Mater. Electron.*, 2018, **29**, 16932-16938.
11. X. Chen, X. Qu, J. Chen and D. Zheng, *High Perform. Polym.*, 2021, **34**, 273-281.
12. C. Fu, C. Yan, L. Ren, X. Zeng, G. Du, R. Sun, J. Xu and C.-P. Wong, *Compos. Sci. Technol.*, 2019, **177**, 118-126.
13. Y. Wang, W. Wu, D. Drummer, C. Liu, W. Shen, F. Tomiak, K. Schneider, X. Liu and Q. Chen, *Mater. Des.*, 2020, **191**, 108698.
14. Z.-B. Zhao, J.-D. Liu, X.-Y. Du, Z.-Y. Wang, C. Zhang and S.-F. Ming, *Colloid Surf. A-Physicochem. Eng. Asp.*, 2022, **635**, 128104.
15. Z. Su, H. Wang, J. He, Y. Guo, Q. Qu and X. Tian, *ACS Appl. Mater. Interfaces*, 2018, **10**, 36342-36351.
16. S. Lee, Y. Kim, D. Park and J. Kim, *Compos. Commun.*, 2021, **26**, 100796.